Orbital-Engineering based Screening of π-Conjugated d^8 Transition-Metal Coordination Polymers for High-Performance *n*-Type Thermoelectric Applications

Wen Shi,[†] Gang Wu,[†] Xue Yong,[†] Tianqi Deng,[†] Jian-Sheng Wang,[‡] Jin-Cheng Zheng,[§] Jianwei Xu,[#] Michael B. Sullivan,[†] and Shuo-Wang Yang[*,†]

[†]Institute of High Performance Computing, Agency for Science, Technology and Research, 1 Fusionopolis Way, #16-16 Connexis, Singapore 138632
[‡]Department of Physics, National University of Singapore, Singapore 117551
[§]Department of Physics, and Collaborative Innovation Center for Optoelectronic Semiconductors and Efficient Devices, Xiamen University, Xiamen 361005, China
[#]Institute of Materials Research and Engineering, Agency for Science, Technology and Research, 2 Fusionopolis Way, #08-03 Innovis, Singapore 138634

KEYWORDS: *thermoelectric, conducting polymers, first-principles calculations, orbital-engineering, transition-metal coordination polymers*

ABSTRACT: Extraordinary progress has been achieved in polymer-based thermoelectric materials in recent years. New emerging π-conjugated transition-metal coordination polymers are one of the best *n*-type polymer-based thermoelectric materials. However, the microscopic descriptions on geometric structures, orbital characteristics and the most importantly thermoelectric properties remain elusive, which has seriously hampered the experimentalists to

draw a straightforward design strategy for new *n*-type polymer-based thermoelectric materials. Herein, we assess the *n*-type thermoelectric properties of 20 π-conjugated d^8 metal center coordination polymers and rationalize their thermoelectric properties in terms of molecular geometry, orbital nature and electron-phonon coupling based on first-principles calculations. An explicit screening rule for high-performance *n*-type π-conjugated transition-metal coordination polymeric thermoelectric materials was found, *i.e.*, the smaller metal center *d* orbital component ratio in the conduction band minimum, the weaker electron-phonon coupling, the higher intrinsic mobility and thereby the higher thermoelectric power factor can be achieved. Guided by this rule, poly(Pd-C_2S_4) and poly(Ni-C_2Se_4) show very high power factors. We built a map of high-performance π-conjugated transition-metal coordination polymers for *n*-type thermoelectric applications, which will help to accelerate the screening and design of innovative *n*-type thermoelectric polymers.

1. Introduction

Thermoelectric (TE) materials, which can directly generate electricity from heat for power generation via Seebeck effect or convert electricity to heat via Peltier effect for refrigeration, play an important role in relieving environmental and energy problems. The performance of a TE material is determined by a dimensionless figure of merit, $zT = (S^2\sigma T)/\kappa$, where S, σ, κ and T are the Seebeck coefficient, electrical conductivity, total thermal conductivity and the average absolute temperature of the hot and cold junctions, respectively. In solid matter, both electrons and phonons are heat carriers, so the total thermal conductivity is expressed as $\kappa = \kappa_e + \kappa_L$, where κ_e and κ_L are electronic and lattice thermal conductivity, respectively. However, developing highly-efficient TE materials is a challenging task, because these parameters are interrelated and conflicts with each another. For instance, increasing Seebeck coefficient

decreases conductivity, while increasing conductivity enhances electronic thermal conductivity.[1] Engineering the band structures and suppressing the lattice thermal conductivity are believed to be the most successful strategy to enhance *zT*.[2]

Significant progress has been achieved in *p*-type polymer-based TE materials.[3-5] They are flexible, biocompatible, easy to process and possess relatively low lattice thermal conductivity, which makes them superior to conventional inorganic TE materials.[6] The development of high-performance *n*-type TE polymers is quite challenging, but very recently, polymer-based *n*-type TE materials with outstanding performance have been emerging,[7,8] such as transition-metal coordination polymers,[9] ladder-type conducting polymers,[10] *etc*. Among them, π-conjugated transition-metal coordination polymers are one of the best *n*-type polymer-based TE materials.[9] For example, poly(nickel-ethylenetetrathiolate), *i.e.*, poly(Ni-C_2S_4) powder shows a high *zT* value of 0.2 at 440 K,[11] and its *zT* can even reach up to 0.32 in its films with conductivity of 310 S cm^{-1}, Seebeck coefficient of −150 μV K^{-1} and total thermal conductivity of 0.8 W m^{-1} K^{-1} at 400 K.[12] However, the mechanism behind such high performance remains unclear, and the microscopic descriptions of geometric structure, electronic properties and the most importantly TE transport process in general are far from being complete due to polymeric complex morphologies. Therefore, understanding the relationship of TE property with molecular geometry and electronic structure at the atomistic level is highly demanded and really urgent, where theoretical investigations can provide extremely important information. As far as we know, theoretical explorations on the *n*-type TE properties of π-conjugated transition-metal coordination polymers have never been reported before.

In this work, we study the intra-chain *n*-type TE properties of 20 π-conjugated d^8 transition-metal coordination polymers and elucidate the relations of their TE performance to the polymer

backbone configurations, electronic structures and electron-phonon coupling using density functional theory (DFT). It is found that the *p* orbitals of coordination atoms and carbon atoms in the linking bridge contribute approximately 80% to the conduction bands (CB); more importantly, less metallic *d* orbital component ratio at the conduction band minimum (CBM) weakens the electron-phonon coupling and thus increases the intrinsic mobility and eventually enhance the TE power factor. Guided by this screening rule, poly(palladium-ethylenetetrathiolate) [poly(Pd-C_2S_4)] and poly(nickel-ethylenetetraselenol) [poly(Ni-C_2Se_4)] are predicted to have the highest power factors among these 20 polymers. Additionally, we demonstrated that the intrinsic electron-phonon scatterings in these ladder-like coordination polymers are dominated by longitudinal-acoustic phonon scatterings at room temperature. These results will be very helpful for the experimentalists in screening and designing new high-performance *n*-type polymer-based TE materials.

2. Computational Methods

2.1 Electronic structure calculations. In a real polymer thin film, both crystalline and amorphous regions are present. For the crystalline domains, both the intra-chain and inter-chain TE transport processes coexist. Herein, as a first step, we used isolated 'ideal' polymer chains to explore the intra-chain TE transport properties. A more elaborate model including inter-chain TE transport processes is being studied and incorporating amorphous domains will be studied in the future. The polymer backbones lie along the *a*-axis. The unit cell lengths in the in-plane *b* and out-of-plane *c* axes are both fixed at 20 Å. Both the lattice parameters of *a* and ionic positions were optimized by the projector augmented wave (PAW) method[13] with the Perdew-Burke-Ernzerhof exchange correlation functional[14] with the dDsC dispersion correction[15] (PBED) functional in the Vienna ab initio simulation package (VASP).[16] The different functionals have

been performed to optimize the structure for **1** (Table S1). The electronic structure calculations were conducted by the HSE06 functional.[17] The different functionals have been tested to carry out the band structure calculations for **1** (Figure S3 and S4). Throughout the calculations, the convergence criterion of the total energy was set to be 10^{-5} eV in the self-consistent field iteration. The cutoff energy for the plane-wave basis set was set to be 900 eV. The **k**-mesh of 16×1×1 was used during the optimization. The single-point energy and charge density calculations were performed on the **k**-mesh of 32×1×1.

2.2 TE transport coefficients calculations. Boltzmann transport theory[18] was employed to model the TE transport coefficients, including the conductivity, σ, and Seebeck coefficient, S, which can be expressed as

$$\sigma = \frac{e^2}{V}\sum_{\boldsymbol{k}}\left(-\frac{\partial f_0(\varepsilon_{\boldsymbol{k}})}{\partial \varepsilon_{\boldsymbol{k}}}\right)\boldsymbol{v}_{\boldsymbol{k}}\boldsymbol{v}_{\boldsymbol{k}}\tau_{\boldsymbol{k}}\,, \tag{1}$$

$$S = \frac{e}{V\sigma T}\sum_{\boldsymbol{k}}\left(-\frac{\partial f_0(\varepsilon_{\boldsymbol{k}})}{\partial \varepsilon_{\boldsymbol{k}}}\right)(\varepsilon_{\boldsymbol{k}} - \varepsilon_{\mathrm{F}})\boldsymbol{v}_{\boldsymbol{k}}\boldsymbol{v}_{\boldsymbol{k}}\tau_{\boldsymbol{k}}\,. \tag{2}$$

Here $f_0(\varepsilon_{\boldsymbol{k}}) = 1/[\exp((\varepsilon_{\boldsymbol{k}}-\varepsilon_{\mathrm{F}})/k_{\mathrm{B}}T) + 1]$ is the Fermi-Dirac distribution function; ε_{F} is the Fermi energy; V is the volume of unit cell; $\boldsymbol{v}_{\boldsymbol{k}} = (1/\hbar)\nabla_{\boldsymbol{k}}\varepsilon_{\boldsymbol{k}}$ is the group velocity; $\varepsilon_{\boldsymbol{k}}$ is the band energy at a given **k**-point; $\tau_{\boldsymbol{k}}$ is the relaxation time, and $\hbar$ is reduced Planck constant. The group velocity was derived from the first-principles band structure calculations. To estimate the summation in the **k**-space, we applied the Wannier function-based interpolation to obtain the ultra-dense band energies via the wannier90 program.[19] The TE transport coefficients were calculated by revised BoltzTraP program,[20] where relaxation times were obtained from first-principles calculations.[21,22]

2.3 Relaxation time calculations. The relaxation time has the form $1/\tau_{\boldsymbol{k}} = (2\pi/\hbar V)\sum_{\boldsymbol{k}'}|M(\boldsymbol{k},\boldsymbol{k}')|^2\delta(\varepsilon_{\boldsymbol{k}} - \varepsilon_{\boldsymbol{k}'})(1-\cos\theta)$, where θ is the scattering angle, calculated from

first-principles electronic structures. We herein considered the longitudinal acoustic phonon scattering. The DP theory[23] was applied to quantitatively estimate the electron-acoustic phonon scattering, under which, the scattering matrix element takes the form $|M(\boldsymbol{k},\boldsymbol{k}')|^2 = k_{\mathrm{B}}TE_1^2/C_{ii}$, where E_1 is the DP constant and C_{ii} is the elastic constant. The DP theory has proven to be a robust strategy to predict the intrinsic mobility of low-dimensional carbon-based materials,[24] TE properties of doped organic molecular crystals[25] and TE properties of doped crystalline conjugated polymers.[26,27] Both the DP constant and elastic constant were determined from first-principles calculations, and the detailed calculation methods are shown in Section 3 of the SI.

The phonon dispersion, accurate electron-phonon coupling and relaxation time for **1** were calculated by density functional perturbation theory (DFPT)[28] combined with Wannier function interpolation[29]. Phonon dispersion was calculated using norm-conserving pseudopotential[30] with PBE exchange correction functional[14] in QUANTUM ESPRESSO package.[31] The cutoff energy for plane-wave basis set was set to be 80 Ry. The **k**- and **q**-mesh of 16×1×1 were used. Electron-phonon coupling and phonon dispersion were interpolated into a finer mesh using maximally localized Wannier functions through Electron-Phonon coupling using Wannier functions (EPW) program.[32] The electron relaxation time was evaluated through the relation $\tau_{\boldsymbol{k}} = -\hbar/[2\ \mathrm{Im}(\Sigma_{\boldsymbol{k}})]$, where $\mathrm{Im}(\Sigma_{\boldsymbol{k}})$ is the imaginary part of Fan-Migdal quasiparticle self-energy.[33]

3. Results and Discussion

3.1. Polymer backbone structure resolution.

20 coordination polymers studied in this work are given in Figure 1a, where **1**-**3**, **5** and **6** are constructed with tetrathiooxalate-like linking bridges (C_2S_4, C_2Se_4, C_2Te_4) and Ni or Pd metal centers, respectively; while **4** is a Ni-tetraimine coordination. **7**-**9** possess a dithiocarbamate-like coordination geometry and they are the isomers of **1**, **2** and **5**, respectively. The calculated

binding energy for **1** is 0.11 eV/atom lower than that of **7** [Table S1 in Supporting Information (SI)], indicating that the dithiolene coordination geometry is more favorable than the dithiocarbamate one. This agrees with the previous theoretical calculations by Hoffmann *et al.*, who claimed that both dithiolene and dithiocarbamate coordination modes should be stable based on extended Hückel methodology; nevertheless, the dithiolene-like coordination is more stable.[34] **10** is poly(Ni-tetrathiosquarato) [poly(Ni-ttsq)]. **11**-**13** consist of quinoid-like moieties in their ligands, namely 1,4-dithiins, 1,4-dioxin and 1,4-dimethylpyrazine; and **14**-**17** contain either benzene or hetero-aromatic rings including thiophene, furan and pyrrole. While, **18** and **19** have multiple thiophenes fused with one and two benzene ring(s) in their ligands. **20** is poly(Ni-tetrathiofulvalenetetrathiolate) [poly(Ni-ttftt)].

All these polymer backbones have a planar configuration and their optimized structural parameters are given in Figure S1 and Table S1. Using the extended X-ray absorption fine structure technique, experimentalists have characterized **1**, where the bond lengths of Ni-S, C-S, and C-C are 2.169 Å, 1.75 Å and 1.35 Å; and the bond angles of S-Ni-S and Ni-S-C are 95° and 103°, respectively,[35] which are well reproduced by our calculations at PBED level (Table S1). In these 20 polymers, the metal centers, Ni and Pd are typical d^8 electron transition-metals, and their dsp^2 hybridization shows a square-planar configuration when four ligands coordinated. The ligands in these structures consist of π-conjugated fragments without rotatable single bonds, making them highly rigid and thereby facilitating the extension of electron conjugation along the polymer chains (Figure 1b), which promotes the high intra-chain charge transport properties. A wide variety of organic ligands and metal centers in these polymers provides considerable chemical tunability in the electronic structure, charge transport and TE property.

Generally, the coordination bond lengths depend on the size of coordination atoms and metal centers. For example, the coordination bond lengths increase from **1** to **3** (2.154 Å, 2.270 Å and 2.440 Å) as van der Waals (vdW) radii increase from 1.80 Å (sulphur) to 1.90 Å (selenium) and 2.06 Å (tellurium). The shortest bond length is found in **4** because nitrogen has the smallest vdW radius of 1.55 Å (Table S1). However, the situation is different when the coordination configurations become different. For example, the coordination bond lengths in **7**-**9** (2.202 Å, 2.314 Å and 2.348 Å for **7**-**9**) are longer than that in **1**, **2** and **5** because of the strong repulsion of the lone-paired electrons on the two coordination atoms in four-membered rings. Meanwhile, no significant change of Ni-S distances is found in **10**-**20** (Table S1).

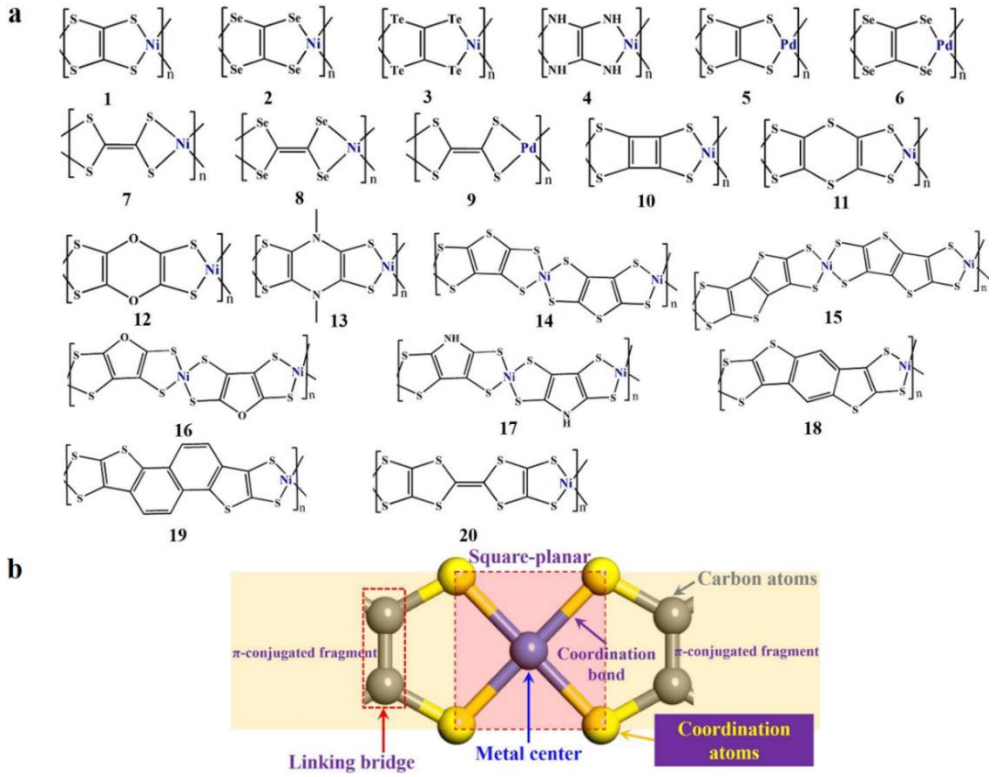

Figure 1. (a) The chemical structures of 20 π-conjugated d^8 transition-metal coordination polymers studied in this work. (b) Schematic illustration of coordination geometry of these polymers, in which the d^8 metal centers show a square-planar coordination geometry. The metal

centers, coordination atoms and carbon atoms in the linking bridges are represented in blue, yellow and grey, respectively.

3.2. Electronic structure characteristics.

It can be found that the band gaps increase when the electron effective mass increases (Figure 2a), because the repulsion between CB and valence bands (VB) increases the band curvature. Mahan has proven that the band gap of a potential TE material should be larger than $10k_BT$, namely around 0.26 eV at room temperature so as to avoid the bipolar effects on the Seebeck coefficients, which attenuates the Seebeck coefficients significantly.[36] We do observe the bipolar effect on Seebeck coefficient for **2**, **11**-**12**, **14**-**17** and **20**, and we will discuss it in the section of 'TE properties' in detail. The band gaps of the rest coordination polymers are much larger than $10k_BT$, which effectively avert the bipolar effects on the reduction of Seebeck coefficients. On the contrary, the larger band gaps result in heavier effective mass as show in Figure 2a, which inevitably leads to low mobility. Fortunately, nine polymers, **1**, **5**-**9**, **13** and **18**-**19** exhibit modest band gaps and small effective masses, which implies good charge transport and TE properties. To obtain the insight of structural effects, we plot the atomic orbital component ratios within CB (Figure 2c), including the orbitals of coordination atoms (S, Se or Te), carbon atoms in the linking bridges and metal centers (Ni or Pd). It is noted that the p_z orbitals of 4-fold coordination atoms and carbon atoms in linking bridges and the d_{xz} orbital of one metal center contribute approximately 90% to the CB; among them the p_z orbitals of coordination atoms possess about 49%; carbon atoms 32% and metal d_{xz} 12%, respectively. Therefore, to effectively engineer the electronic structures for good charge transport and thereby TE properties, modifying these atoms is an efficient way.

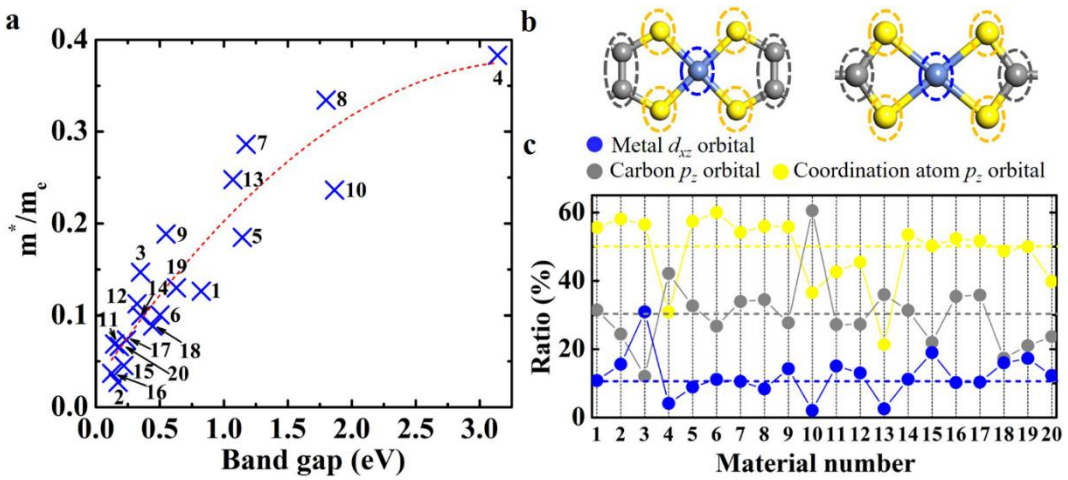

Figure 2. (a) The relation between electron effective mass, m^*/m_e and band gap. The red dashed curve shows the trend. The detailed data are given in Table S2. (b) The important atoms, that is, coordination atoms, carbon atoms in the linking bridges and metal centers. (c) The atomic orbital component ratios contributed to CB, including the orbitals of coordination atoms, carbon atoms in the linking bridges and the metal centers highlighted in the dashed line circles in Figure 2b. The dashed lines in Figure 3b represent the averaged ratios for these twenty polymers. The detailed data for electron effective masses, band gaps and atomic orbital component ratios at CB are summarized in Table S3.

In general, the strength of *p*-*d* orbital coupling between the π-conjugated fragments and metal centers can be expressed as $V_{pd} = \langle p|\Delta V|d\rangle^2/(\varepsilon_p - \varepsilon_d)$, where ΔV is the coupling potential and $(\varepsilon_p - \varepsilon_d)$ is the energy difference between the *p* and *d* orbitals. Due to the relatively high energies of *d* orbitals, the energy differences between metallic *d* orbitals and conjugated fragment *p* orbitals are small, which results in strong *p*-*d* interactions, *i.e.* strong π-*d* interactions in these coordination polymers.[37] That is the reason for **1**-**6** exhibiting wide CB bandwidths (Figure 3), meaning the electron delocalization and thereby decent charge transport properties. In addition, **1**-**6** are direct band gap semiconductors (Figure 3) and all of them show small electron

effective masses around 0.03~0.38m_e (see Figure 2a and Table S2). Using angle resolved photoemission spectroscopy, it has been verified that highly aligned semicrystalline conjugated polymers, like cyclopenta [2,1-b:3,4-b']dithiophene pyridyl[2,1,3]-thiadiazole (PCDTPT) show electron delocalized characteristics and have extremely small hole effective mass of 0.106m_e along the polymer chain direction at room temperature.[38] Such hole effective mass is smaller than the conduction band effective masses (0.97m_e, 0.19m_e, 1.08m_e and 0.26m_e for longitudinal, transverse, density of state and conductivity effective masses, respectively) and valence band effective masses (0.61m_e and 0.16m_e, for density of state and light-hole effective masses, respectively) of silicon single crystal.[39] Compared with PCDTPT, our calculated electron effective masses for **1, 3**-**6** are of the same order of magnitude and even one magnitude smaller for **2** (Table S2), indicating their electron delocalized nature. Meanwhile, **1** and **2** have almost the same CB bandwidths (1.40 eV), but **3** shows a small CB bandwidth (0.84 eV). This is because the longer Ni-Te bonds (2.440 Å) and C-Te bonds (2.093 Å) attenuate the *p*-*d* and *p*-*p* interactions. The CB bandwidths of **5** and **6** are almost the same (1.07 eV for **5** and 1.08 eV for **6,** respectively), but **6** exhibits a narrower band gap (0.50 eV) than **5** (1.14 eV). Besides, due to the larger electronegative difference between Ni and N atoms, **4** has a wide band gap (3.14 eV) (Figure 3 and Table S2). Except for **4** in **1**-**6**, **1**-**3**, **5**-**6** possess relatively low LUMO level (–6.0~–5.4 eV), namely large electron affinity (Table S2). Currently, the experimental reported electron affinity of the state-of-the-art *n*-type organic semiconductor, 2,3,5,6-tetrafluoro-7,7,8,8-tetracyanoquinodimethane (F_4-TCNQ) is 5.08 eV,[40] which is still a little bit higher than our calculated values for **1**-**3**, **5** and **6**. Such unique features facilitate these coordination polymers to realize *n*-type TE properties easily.

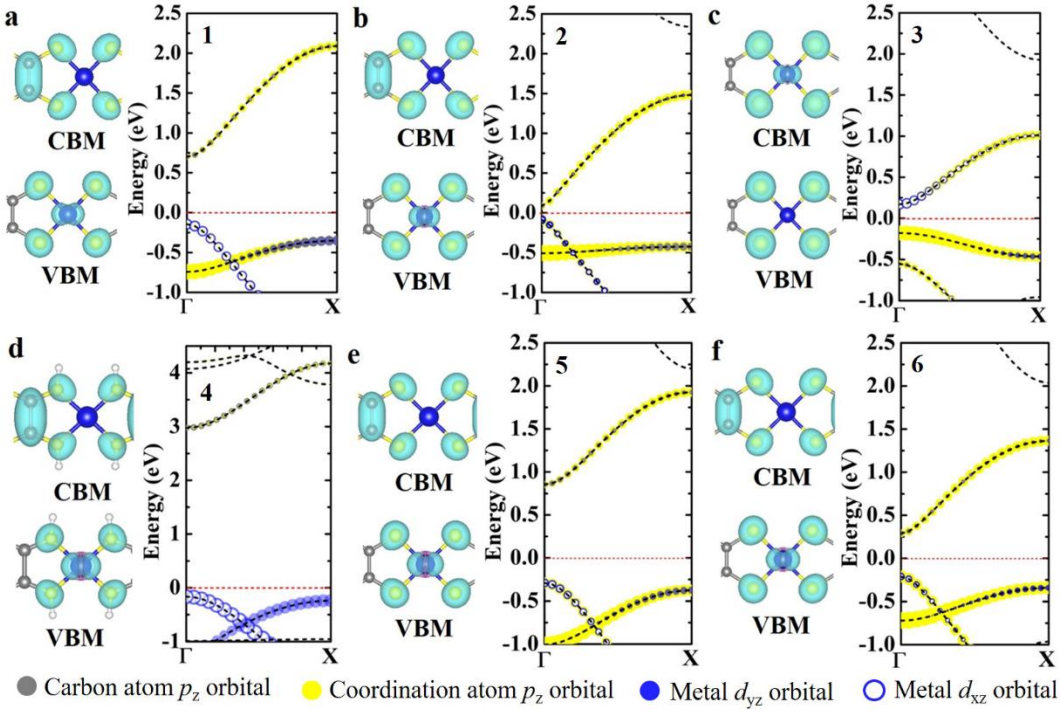

Figure 3. (a)-(f) Orbital-projected band structures and charge density isosurfaces for **1**-**6**, respectively. The symbol size shows the relative weight of the component ratio. The non-orbital-projected band structures are displayed in the black dashed lines and red dashed lines are the Fermi energy levels. The reciprocal coordinates of high-symmetry k-points in the first Brillouin zone are Γ = (0, 0, 0) and X = (0.5, 0, 0). The band structures of the rest 14 coordination polymers are shown in Figure S5 and S6; and their charge density isosurfaces are presented in Figure S7 and S8. The detailed data of bandwidths, band gaps and LUMO energy levels are summarized in Table S2. Band structures calculated by LDA, PBE, PBE+U, B3LYP, HSE06 and HSE06 with spin polarization for **1** are displayed in Figure S3. Band structures calculated by PBE+U with different U values for **1** are displayed in Figure S4. The electron localization function map and Bader charge analysis for **1** are shown in Figure S9.

Compared with above tetrathiooxalate structures, **7**-**9** have smaller CB bandwidths (0.99, 1.04 and 0.82 eV for **7**, **8** and **9**, respectively) due to their longer coordination bonds (Table S1),

which weaken the π-d interaction. **10** is a semiconductor with direct band gap of 1.87 eV (Figure S5 and Table S2). While, **11-13** containing the quinoid-like fragments, show very different band structures (Figure S5) and their CB bandwidths narrow down to 0.50~0.60 eV, because the quinoid-like moieties are averse to the conjugation along backbones. Very similar band structures were found for **14-17** (Figure S6), and they all show narrow CB bandwidths as the p_z orbitals of heteroatoms in thiophene, furan or pyrrole contribute little to the CB (Table S3). **20** is a narrow band gap semiconductor having a very small CB bandwidth (0.38 eV) (Figure S6 and Table S2). We can see that introducing aromatic or quinoid-like moieties in the ligands does not benefit the CB bandwidth-widening, but increases the metal centers d_{xz} orbital ratios at CBM (Figure S7 and S8). This is because those aromatic or quinoid-like fragments are electron attractive which shift down the LUMO levels closer to the metal d_{xz} orbital level.

3.3. Electron-phonon coupling.

It is well known that the intrinsic charge transport is limited by the inherent lattice vibration in a perfect crystal. Based on DFPT[28] combined with Wannier function interpolation[29], we conducted the electron-phonon coupling calculations for **1**. From the accumulative scattering rate (Figure 4a), it is very interesting to find that about 89% contribution of electron scattering is derived from the phonon modes with energy lower than 2.0 meV at room temperature, which means that the low-energy acoustic phonon plays a dominant role in the charge transport process. Furthermore, our calculated room-temperature electron relaxation time by deformation potential (DP) theory[23] is 290 fs, which is very close to the calculated value considering all phonon modes scattering (202 fs). This clearly demonstrates again that the acoustic phonon scattering governs the charge transport process at room temperature.

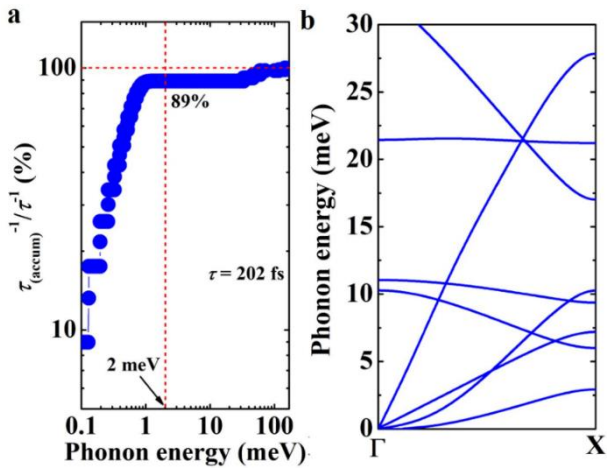

Figure 4. (a) The ratio of accumulative scattering rate, $\tau_{(accum)}^{-1}$ to total scattering rate, τ^{-1} for **1** at room temperature. Scattering rate accumulation function is expressed as $\tau_{(\mathrm{accum})}^{-1}(\varepsilon) = \sum_{\boldsymbol{q},\lambda}^{\hbar\omega_{\boldsymbol{q}} \leq \varepsilon} \tau_{\boldsymbol{q},\lambda}^{-1}$, which identifies the scattering rate due to phonons with energy smaller than ε. The horizontal dashed red line shows 100%. The vertical dashed line shows the phonon energy of 2 meV. (b) Phonon dispersion for **1**. Phonon dispersion with all branches and projected phonon density of states are displayed in Figure S10.

Based on DFPT combined with Wannier function interpolation, Shuai *et al.* have shown that the intrinsic electron-phonon scatterings in two-dimensional carbon-based materials are dominated by the low-energy longitudinal-acoustic phonon scatterings in the temperature range of 10 K to 600 K.[41] It was also demonstrated that the acoustic phonon scattering intensities in oligoacene single crystals are larger than that caused from optical phonon, and the calculated mobility matched better with the experimental results for ultrapure single crystals.[42] Besides, Bardeen and Shockley also provided a simple criterion to justify the dominant role of acoustic phonon in the charge transport process. At room temperature, the electron energy is around 26 meV (~ $k_B T$), corresponding to its velocity of 10^5 m s^{-1}. In this context, the de Broglie wavelength is about 70 Å, and the energy of a phonon of corresponding wavelength is about 2 meV, which is the

acoustic phonon in the long wavelength limit.[23] According to the phonon dispersion of **1** (Figure 4b), we can find that the optical branches with the lowest energy locate around 6 meV, higher than 2 meV, so such optical branches cannot scatter the electron effectively. Therefore, for this series of polymers, it is reliable to consider the longitudinal acoustic phonon scatterings to calculate the charge transport and TE properties based on the DP theory.[23]

In DP theory, DP constants and elastic constants are the two pivotal physical quantities to describe the electron-phonon coupling quantitatively. Our calculated electron DP constants and elastic constants are summarized in Table S4. It can be seen that smaller component ratios of d_{xz} orbitals from metal centers at the CBM result in smaller electron DP constants, which significantly depress electron-phonon coupling (Figure 5a). Furthermore, we use the tight-binding model to qualitatively uncover the relation between the electron DP constants and metal centers d_{xz} orbital component ratios at CBM. The detailed derivation is given in Section 4 of SI. A unit cell of coordination polymers in our study can be represented as a Hamiltonian, $H = \varepsilon_d a_d^\dagger a_d + \varepsilon_p a_p^\dagger a_p + (t_{pd}/2) a_d^\dagger a_p + (t_{pd}^*/2) a_p^\dagger a_d$, where $a_{d,p}^\dagger$ and $a_{d,p}$ are the creation and annihilation operators on d (metal center) and p (π-conjugated fragment) sites, respectively; $\varepsilon_{p,d}$ and t_{pd} are the corresponding on-site energy and the p-d inter-site electronic coupling for measuring the p-d orbital coupling strength. So the absolute value of DP constant can be represented as $|E_1| = \underbrace{\frac{1}{(1-k_{pd}/k_{pp})(2/a)+(k_{pd}/k_{pp})(1/r)}}_{(1)} \underbrace{\sqrt{w_d(1-w_d)}}_{(2)} \underbrace{\left|(dt_{pd}^{\mathrm{eff}}/dr)\right|}_{(3)}$. Here, k_{pd} and k_{pp} are the local elastic constants of d-p sites and p-p sites, respectively; r, a and w_d are the d-p inter-site distance, the lattice parameter and the metal center d orbital component ratio at CBM, respectively. $t_{pd}^{\mathrm{eff}} \propto t_{pd}$ is the periodic effective p-d inter-site electronic coupling, and the detailed description of this parameter is given in Section 4 of SI. Accordingly, the DP constant is

determined by three terms. Term-(1) reflects the influence of polymer backbone geometry and bond stiffness. Term-(2) shows the *d* orbital contribution. It is clear that a small fraction of *d* orbital contribution, w_d will result in a small DP constant, which is exactly what we have observed in Figure 5a. Term-(3) reflects electron-phonon coupling, mainly determined by the *p*-*d* electronic coupling in these coordination polymers. Combining the first and the third terms, we can understand the larger *r/a* ratio, the small DP constant, which requires large radius of transition-metal center and short organic ligand, like **1**-**6**. The derivation is given in Section 4 of SI.

It is noted that the DP constants of **1**-**2**, **4** and **6** are very close (2.248 eV, 1.862 eV for **1**-**2**, and 1.795 eV, 2.175 eV for **4**, **6**); but **3** shows a larger DP constant (4.537 eV) due to its obvious Ni d_{xz} orbital ratio at the CBM (Table S3 and S4). Interestingly, **5** has an ultra-low DP constant (0.2881 eV) because of the large deformation of Pd-S coordination bond (0.55%); meanwhile, Pd d_{xz} orbital has no contribution to the CBM (Table S3 and S5). This implies its weak electron-phonon coupling in polymeric backbone and thereby excellent charge transport properties. Besides, **7**-**9** also show small DP constant (0.2185 eV, 0.8672 eV and 0.3426 eV for **7**-**9**, respectively) and the reason is the same as that in **5**.

The gradual decrement in elastic constants in **1**-**6** (1.592 for **4**, 1.183 for **1**, 1.080 for **5**, 1.060 for **2**, 0.9470 for **3**, and 0.8577 for **6**, unit: $\times 10^{-7}$ J m^{-1}, Table S4) is due to the increment of vdW radii of coordination atoms or ionic radii of metal centers, *i.e.*, the increment of coordination bonds (Table S1). It suggests that the polymeric chain stiffness can be engineered via the substitutions of metal centers or coordination atoms. By the way, these 20 coordination polymers are much more rigid than polyguanylic acid, but are as rigid as graphdiyne nanoribbons. Because the calculated elastic constants for these ladder-like coordination polymers (0.8-2.5$\times 10^{-7}$ J m^{-1})

are much larger than those for polyguanylic acid (4.36×10^{-10} J m^{-1}),[43] but comparable with those for graphdiyne nanoribbons ($1.66\text{-}2.99\times10^{-7}$ J m^{-1}) (Table S4).[44] Such rigid ladder-like backbones for these coordination polymers warrant the high intra-chain charge transport properties.

In addition, we can see that the smaller d_{xz} orbital component ratio at CBM, the smaller DP constants, and eventually the longer mean electron relaxation times (Figure 5b). The electron relaxation times of **5**, **7** and **9** (4,698 fs, 3,332 fs and 1,340 fs) are one or two order(s) of magnitude higher than those of the rest structures, which attributes to their ultra-low DP constants. The relaxation time for a perfect graphene can reach up to 20 ps at room temperature verified by the cyclotron resonance response technique;[45] yet this value is still one order of magnitude higher than our calculated values for **5**, **7** and **9**. Besides, the electron relaxation times of **1**-**2**, **6**, **8**, **10** and **14**-**19** fall in hundreds femtosecond, and **3**-**4**, **11**-**13** and **20** in dozens femtosecond (Table S4).

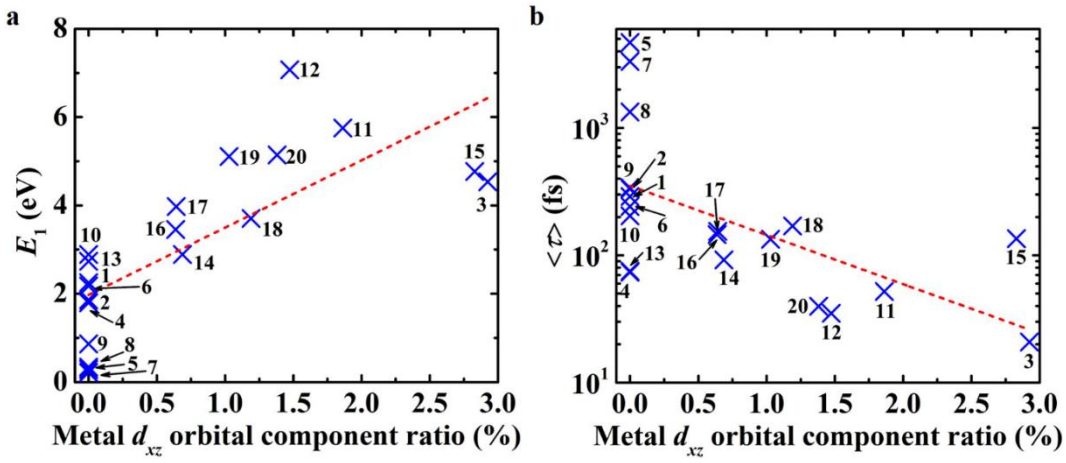

Figure 5. (a) The trend of electron DP constants, E_1 *vs.* d_{xz} orbital component ratios within CBM. (b) The trend of mean electron relaxation times, $<\tau>$ *vs.* metal center d_{xz} orbital component ratios within CBM at 298 K. The logarithmic mean relaxation times are shown in the ordinate. The detailed data for electron DP constants and mean relaxation times are summarized in Table S4.

3.4. Intrinsic mobility.

The intrinsic charge carrier mobility, μ, is a crucial measureable quantity to determine the TE properties for a material because larger mobility means higher conductivity at a given carrier concentration as $\sigma = \mu eN$, where e is the elementary charge, and N is the carrier concentration. Intrinsic mobility is dependent on relaxation time, which is a quantitative index of electron-phonon coupling. Long relaxation time leads to large mobility (Figure 6a) owing to the relation $\mu = e < \tau > / m^*$. Due to the small differences in electron effective mass for these coordination polymers (Figure 2a), the electron-phonon coupling plays the dominant role in the charge transport properties.

In detail, **1**-**2**, **6**, **8**-**10** and **14**-**19** show excellent mobilities (~ 10^3 cm^2 V^{-1} s^{-1}), while for **3**-**4**, **11**-**13**, and **20**, the mobilities are one order of magnitude lower (Figure 6a and Table S4). To date, the experimental measured mobility for such coordination polymers is still unavailable. But an extremely high field-effect mobility (116 cm^2 V^{-1} s^{-1} for electrons and 99 cm^2 V^{-1} s^{-1} for holes) at room-temperature for a highly crystalline films of π-conjugated copper coordination polymer, Cu-BHT (BHT = benzenehexathiol) was reported.[46] Moreover, the intra-chain hole mobilities of isolated ordered ladder-like poly(p-phenylenes) chains are found to be close to 600 cm^2 V^{-1} s^{-1} at room temperature based on time resolved microwave conductivity measurement.[47] Our predicted electron mobilities for **3**-**4**, **11**-**13**, and **20** are close to these two experimental observations, suggesting that these planar π-conjugated transition-metal coordination polymers should have prominent electron mobility as well. Among these 20 polymers, **5** and **7** possess the highest mobility (6.38×10^4 cm^2 V^{-1} s^{-1} for **5** and 2.00×10^4 cm^2 V^{-1} s^{-1} for **7**, respectively) due to their large CB dispersion and the most importantly the very weak electron-phonon couplings. The

calculated electron mobilities for **5** and **7** are comparable with graphdiyne nanoribbons at room temperature (~ 10^4 cm^2 V^{-1} s^{-1}).[44]

In this work, we adopted an 'ideal' crystal model for these ladder-like coordination polymers and employed Boltzmann transport theory assuming the electronic properties can be described by the delocalized bands. In view of many cutting-edge experimental[48] and theoretical[49] studies, near room temperature the band transport behavior dominates the charge transport process in crystalline or highly-oriented polymer-based materials, such as those used in this work. Because the electrons in the highly oriented conducting polymers shows delocalized behavior at room temperature,[38,50-52] and the room-temperature measured mobilities for some highly aligned polymers are close to 100 cm^2 V^{-1} s^{-1},[53,54] and the highest reported value is 600 cm^2 V^{-1} s^{-1}.[47] Moreover, band-like mobility-temperature relations are detected in many different highly aligned conjugated polymers.[55-57] More detailed discussions on the validity of our theoretical framework can be found in Section 5 of SI.

3.5. TE properties.

Herein, we adopted the rigid band approximation to simulate the doping effect. By shifting Fermi energy, Seebeck coefficient and conductivity can be presented as a function of electron concentration. The calculated Seebeck coefficients of 1 decay linearly with the logarithm of the electron concentrations, while the conductivity increases with the electron concentration shown in Figure S14. Consequently, a peak value of power factor appears at around 9.8×10^{20} m^{-3}, denoted as the optimal electron concentration. The electron concentration dependent TE properties of these 20 polymers, *i.e.*, the optimal electron concentration, the corresponding room-temperature Seebeck coefficients, conductivities and peak value of power factors are given in Table 1. We can see that the optimal electron concentrations for these 20 polymers are in the

range of 10^{20}-10^{21} cm^{-3} and their Seebeck coefficients fall in the range of −80 to −210 μV K^{-1}, which is quite accordant with the experimental measured value for poly[K_x(Ni-C_2S_4)], *i.e.* −125 μV K^{-1} at room temperature.[12] However, the conductivities of these polymers fluctuate wildly from 10^4 to 10^7 S cm^{-1}, mainly due to the large difference in their mobilities. It was reported that the conductivity of poly[K_x(Ni-C_2S_4)] powder is 40 S cm^{-1} at room temperature,[11] and it can be elevated six times higher to 230 S cm^{-1} by improving the structure-ordering in its films; while its Seebeck coefficients almost remain the same level, implying the mobility enhancement.[12]

We believe that the experimentally measured low conductivities for π-conjugated transition-metal coordination polymers are mainly due to their low carrier concentrations and poor mobilities. In reality, realization of effective high carrier concentration in semiconducting polymers is a challenge owing to their poor chemical doping efficiency.[58] Moreover, the morphology of the experimentally prepared samples is amorphous, adopting coiled configurations with chain entanglements and folding, which localizes the charge carriers and significantly depresses the mobilities. High conductivity for coordination polymers could be achievable once the structural ordered degrees are improved. Liquid-liquid interfacial synthesis technique[59] and the liquid-bridge-mediated nano-transfer printing with vapor phase polymerization method[54] were proven to be extraordinary powerful ways for preparing the highly ordered polymers. It has been experimentally demonstrated that the room-temperature conductivity of poly(3,4-ethylenedioxythiophene) thin films can be improved significantly from 0.007 S cm^{-1} to 1500 S cm^{-1} at the same doping level by improving the structural order.[60] Due to the difficulty in polymerization, some of these coordination polymer samples are often oligomers with an averaged degree of polymerization of range 3-8 only.[61,62] Experimentalists have proven

that the molecular weight plays a key role in improving the mobilities as crystallinity can be improved with growing molecular weight.[63]

The carrier concentration dependent TE properties are very important for TE materials, especially the peak value of the power factor at the optimal carrier concentration. Thereby in the following, we focus on the peak value of power factors of these 20 polymers and try to bridge the gap between the intrinsic transport properties of a material and the carrier concentration dependent power factor. It is found that the peak value of power factors increases with intrinsic relaxation times increasing, and the underlying mechanism is the increment of intrinsic mobility (Figure 6b). Among these 20 polymers, **5** possesses the highest peak value of power factor at room temperature because of its ultra-high intrinsic mobilities (Figure 6a) benefitting from its ultra-weak electron-phonon coupling. In addition, **1**-**2**, **6**, and **7**-**9** also show high peak values of power factor (~ 10^6 μW m^{-1} K^{-2}) and the rest of coordination polymers are around 10^5 μW m^{-1} K^{-2} magnitude.

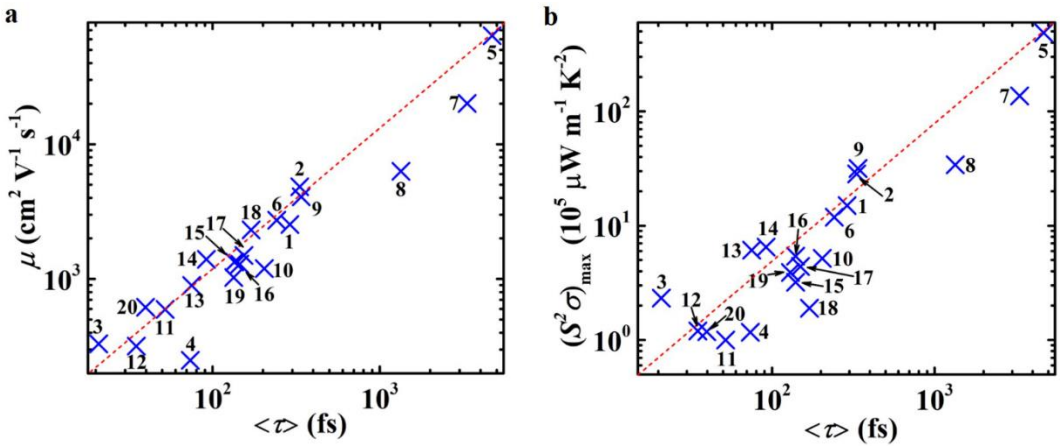

Figure 6. (a) The relation between the intrinsic electron mobility, μ and mean relaxation time, $<\tau>$. The logarithmic mobility and mean relaxation time are shown in the ordinate and abscissa, respectively. The detailed data for electron mobilities are summarized in Table S4. (b) The relation between the peak value of power factor, $(S^2\sigma)_{max}$ at the optimal electron concentration

and mean relaxation time, $<\tau>$. The logarithmic maximum power factor and mean relaxation time are shown in the ordinate and abscissa, respectively. The detailed data for Seebeck coefficients, conductivities and peak value of power factors at optimal electron concentration are given in Table 1.

Table 1. Optimal electron concentration, N_{opt} and the related *n*-type TE properties, including Seebeck coefficient, S, conductivity, σ and power factor, $S^2\sigma$ at 298 K.

Compound	N_{opt} (10^{20} cm^{-3})	S (μV K^{-1})	σ (10^5 S cm^{-1})	$S^2\sigma$ (10^5 μW m^{-1} K^{-2})
1	9.896	-210.5	5.524	15.16
2	5.286	-175.7	9.191	28.37
3	10.23	-181.2	0.7058	2.320
4	8.590	-183.3	0.3468	1.170
5	13.24	-156.3	199.3	487.0
6	6.862	-182.0	3.582	11.86
7	16.42	-141.8	67.79	136.4
8	13.22	-155.2	13.15	31.69
9	15.00	-143.6	16.57	34.16
10	9.084	-168.4	1.824	5.180
11	13.06	-86.60	1.330	0.9976
12	6.182	-189.8	0.3347	1.210
13	12.22	-171.0	2.088	6.107
14	6.068	-182.7	1.947	6.500
15	5.410	-174.6	1.065	3.250
16	9.039	-111.1	4.355	5.380
17	5.758	-179.4	1.350	4.350
18	7.110	-109.9	2.018	2.440
19	6.176	-188.5	1.099	3.910
20	13.45	-85.95	1.603	1.180

In consideration of the doping dilemma in experiments, we provide the TE transport coefficients at additional three lower electron concentrations of 10^{18}, 10^{19} and 10^{20} cm^{-3} and the

results are given in Table S6. It is seen that **2**, **5** and **7-9** still keep high power factors and **2** shows the best power factors in all concentrations. Although experimentally measured carrier concentrations are not available so far for these coordination polymers, a high room-temperature conductivity up to 1580 S cm^{-1} was detected recently in highly crystalline films of Cu-BHT using standard four-probe method.[46] The high-quality polyacetylene films exhibit ultra-high conductivity of 10^4-10^5 S cm^{-1} after doping with iodine at room temperature.[64,65] Compared with these experimental reports, our predicted conductivities for these coordination polymers (10^3-10^5 S cm^{-1}) are on the same order of magnitude at the electron concentration of 10^{20} cm^{-3} (Table S6). **7-9** exhibit high power factor, but they are less stable as discussed above. So we won't recommend them as potential TE materials.

We have noted that the Seebeck coefficients for **2**, **11-12**, **14-17** and **20** show bipolar effect (Figure S15), because their band gaps are quite small (0.12-0.35 eV). When the electron concentration reaches around 5×10^{20} cm^{-3} (near the optimal electron concentration), **2**, **11-12**, **14-17** and **20** show much smaller Seebeck coefficients than **1** which has a wide band gap of 0.82 eV, (Figure S15).

3.6. General selection rule for high-performance π-conjugated transition-metal coordination TE polymers.

The general Seebeck coefficient, S can be expressed as an integral over one electron energy states,[66] namely$S = -(k_B/e)\int(\varepsilon-\varepsilon_F)\sigma(\varepsilon)/(k_BT\sigma)\,d\varepsilon$, where k_B, e, ε_F and T are Boltzmann constant, elementary charge, Fermi energy and temperature, respectively; $\sigma = \int\sigma(\varepsilon)d\varepsilon$ is the conductivity. In the case of mobile electron in the CB only, the power factor can be expressed as a function of electron concentration, N_e,

$$S^2\sigma = \frac{{k_B}^2}{e}\mu N_e[\ln(N_e/N_{eff})]^2, \quad (3)$$

where μ is the intrinsic mobility and N_{eff} is the effective density of states determined by the intrinsic electronic structure of a material.[25] The condition $\partial(S^2\sigma)/\partial N_{\mathrm{e}} = 0$, gives the general expression for the maximum value of power factor

$$(S^2\sigma)_{\max} = \frac{4{k_{\mathrm{B}}}^2}{e}\mu\exp(\ln N_{\mathrm{eff}} - 2), \quad (4)$$

at the optimal electron concentration $N_{\mathrm{opt}} = N_{\mathrm{eff}}/e^2$, where e is the mathematical constant. The detailed formula derivation is provided in Section 6 of SI.

Based on Equation (3), we can see that a higher intrinsic electron mobility will lead to a higher power factor at all electron concentrations, when effective density of states fixed. In addition, a larger effective density of states also gives rise to a higher power factor. Interestingly, the optimal electron concentration only depends on the effective density of state linearly; but unfortunately, higher effective density of state leads to a higher optimal electron concentration (Figure S16). In practice, low optimal doping levels are desirable as the negative effect of dopants on the charge transport and TE properties can be minimized. According to Equation (4), we can plot the maximum power factor as a function of the effective density of states and intrinsic electron mobility shown in Figure 7, where the peak values of power factors increase linearly along the mobility rising, and the maximum power factor likewise increases with the increment of effective density of states. It is noted that the first-principle calculated peak values of power factors for these 20 polymers are consistent with this trend as well (Figure 7), which further confirm the importance of high intrinsic mobility in these polymers for high peak value of power factor. It is noteworthy that for a given mobility, one can use Figure 7 to estimate the power factor easily. For example, when the mobility is about 1 $cm^2\ V^{-1}\ s^{-1}$ at room temperature (nowadays, it is easy to realize such room-temperature mobility for many conducting polymers), the peak value of power factor can reach up to about $10^2\ \mu W\ m^{-1}\ K^{-2}$ (Figure 7). This value is on

the same magnitude of the recently measured maximum power factor for **1** (453 μW m^{-1} K^{-2}).[12] If the intrinsic mobility of a π-conjugated transition-metal coordination polymer can be enhanced, the maximum power factor will be improved significantly and approach to our predicted results. Thus, we have directly bridged the gap between the intrinsic mobility and peak value of power factor for a TE material.

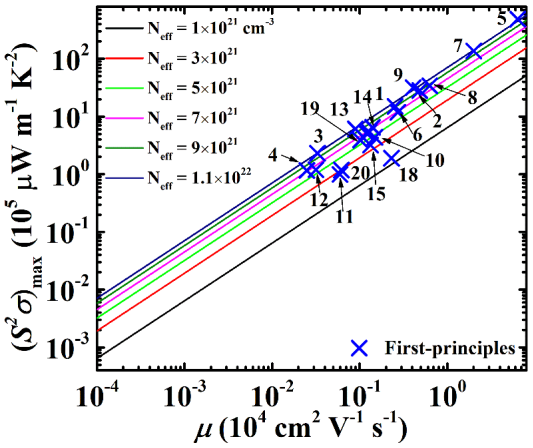

Figure 7. General selection rule for high-performance π-conjugated d^8 transition-metal coordination TE polymers. The dependence of peak value of power factor, $(S^2\sigma)_{max}$ and intrinsic mobility, μ. The first-principles predicted maximum power factor, $(S^2\sigma)_{max}$ for each coordination polymer is labeled as × in the figure. The magnitude of the measured effective density of states for organic semiconductors is usually on the order of around 10^{21} cm^{-3}.[67] The logarithmic maximum power factor and mobility are shown in the ordinate and abscissa, respectively.

Based on the established relations between the peak value of power factor, intrinsic orbital characteristics and electron-phonon coupling, we can thus conclude a general screening rule for high-efficiency π-conjugated transition-metal coordination polymers for *n*-type TE applications, *i.e.* the less metallic *d* orbital component ratio at CBM, the weaker electron-phonon coupling, the higher mobility, and thereby the higher TE power factor. **1**, **2** and **5** meet above selection rule

well, and they are expected to have the best *n*-type TE performance among these 20 coordination polymers.

4. Conclusions

In summary, we studied the TE properties of 20 π-conjugated d^8 transition-metal coordination polymers from first-principles calculations. A screening strategy was proposed to achieve high intrinsic mobility and thereby high *n*-type TE performance, *i.e.*, searching the coordination polymers with minimum metallic *d* orbital component ratio at CBM. This is because the lower *d* orbital component ratio at CBM will weaken the electron-phonon coupling. A weaker electron-phonon coupling leads to a higher intrinsic mobility and thereby a higher peak value of power factor. For these 20 polymers, only the backbones without aromatic and quinoid fragments in the ligands meet the above requirement. Our proposed orbital-engineering-based design criteria for high-performance *n*-type TE polymers can be realized by substitution or modification of coordination atoms, atoms in linking bridges and metal centers, because the *p* and *d* orbitals from these atoms contribute approximately 90% to the conduction bands. According to this screening rule, poly(Pd-C_2S_4) and poly(Ni-C_2Se_4) possess the best *n*-type power factor among these 20 polymers. In addition, we demonstrated that the longitudinal-acoustic phonon scatterings play a dominant role in the electron-phonon scatterings process for these ladder-like coordination polymers at room temperature. We believe that this orbital-engineering approach will help experimentalists to screen and design next-generation π-conjugated transition-metal coordination *n*-type TE polymers.

ASSOCIATED CONTENT

Supporting Information.

The following files are available free of charge.

Supporting computational details, discussions, formula derivations, figures, tables, and supporting references (PDF)

AUTHOR INFORMATION

Corresponding Author

*E-mail: yangsw@ihpc.a-star.edu.sg

Notes

The authors declare no competing financial interest.

ACKNOWLEDGMENT

This work is supported by Agency for Science, Technology and Research (A*STAR) of Singapore (1527200024 and 1527200019). Computational resources are provided by the National Supercomputing Centre Singapore (NSCC) and A*STAR Computational Resource Centre (A*CRC).

REFERENCES

(1) He, J.; Tritt, T. M. Advances in Thermoelectric Materials Research: Looking back and Moving forward. *Science* **2017**, *357*, 1369-1377.

(2) Snyder, G. J.; Toberer, E. S. Complex Thermoelectric Materials. *Nature Mater.* **2008**, *7*, 105-114.

(3) Bubnova, O.; Khan, Z. U.; Malti, A.; Braun, S.; Fahlman, M.; Berggren, M.; Crispin, X. Optimization of the Thermoelectric Figure of Merit in the Conducting Polymer Poly(3,4-ethylenedioxythiophene). *Nature Mater.* **2011**, *10*, 429-433.

(4) Kim, G. H.; Shao, L.; Zhang, K.; Pipe, K. P. Engineered Doping of Organic Semiconductors for Enhanced Thermoelectric Efficiency. *Nature Mater.* **2013**, *12*, 719-723.

(5) Park, T.; Park, C.; Kim, B.; Shin, H.; Kim, E. Flexible PEDOT Electrodes with Large Thermoelectric Power Factors to Generate Electricity by the Touch of Fingertips. *Energy Environ. Sci.* **2013**, *6*, 788-792.

(6) Russ, B.; Glaudell, A.; Urban, J. J.; Chabinyc, M. L.; Segalman, R. A. Organic Thermoelectric Materials for Energy Harvesting and Temperature Control. *Nature Rev. Mater.* **2016**, *1*, 16050-16063.

(7) Bahk, J.-H.; Fang, H.; Yazawa, K.; Shakouri, A. Flexible Thermoelectric Materials and Device Optimization for Wearable Energy Harvesting. *J .Mater. Chem. C* **2015**, *3*, 10362-10374.

(8) Du, Y.; Xu, J.; Paul, B.; Eklund, P. Flexible Thermoelectric Materials and Devices. *Appl. Mater. Today* **2018**, *12*, 366-388.

(9) Zhang, Q.; Sun, Y.; Xu, W.; Zhu, D. Organic Thermoelectric Materials: Emerging Green Energy Materials Converting Heat to Electricity Directly and Efficiently. *Adv. Mater.* **2014**, *26*, 6829-6851.

(10) Suhao, W.; Hengda, S.; Ujwala, A.; Mikhail, V.; Å., P. P. O.; W., A. J.; Walter, T.; Magnus, B.; Xavier, C.; Daniele, F.; Simone, F. Thermoelectric Properties of Solution‐Processed n‐Doped Ladder‐Type Conducting Polymers. *Adv. Mater.* **2016**, *28*, 10764-10771.

(11) Sun, Y.; Sheng, P.; Di, C.; Jiao, F.; Xu, W.; Qiu, D.; Zhu, D. Organic Thermoelectric Materials and Devices based on p- and n-Type Poly(metal 1,1,2,2-ethenetetrathiolate)s. *Adv. Mater.* **2012**, *24*, 932-937.

(12) Sun, Y.; Qiu, L.; Tang, L.; Geng, H.; Wang, H.; Zhang, F.; Huang, D.; Xu, W.; Yue, P.; Guan, Y.-s.; Jiao, F.; Sun, Y.; Tang, D.; Di, C.-a.; Yi, Y.; Zhu, D. Flexible n-Type High-Performance Thermoelectric Thin Films of Poly(nickel-ethylenetetrathiolate) Prepared by an Electrochemical Method. *Adv. Mater.* **2016**, *28*, 3351-3358.

(13) Blöchl, P. E. Projector Augmented-Wave Method. *Phys. Rev. B* **1994**, *50*, 17953-17979.

(14) Perdew, J. P.; Burke, K.; Ernzerhof, M. Generalized Gradient Approximation Made Simple. *Phys. Rev. Lett.* **1996**, *77*, 3865-3868.

(15) Steinmann, S. N.; Corminboeuf, C. A Generalized-Gradient Approximation Exchange Hole Model for Dispersion Coefficients. *J. Chem. Phys.* **2011**, *134*, 044117-044121.

(16) Kresse, G.; Furthmüller, J. Efficient Iterative Schemes for Ab Initio Total-Energy Calculations Using a Plane-Wave Basis Set. *Phys. Rev. B* **1996**, *54*, 11169-11186.

(17) Krukau, A. V.; Vydrov, O. A.; Izmaylov, A. F.; Scuseria, G. E. Influence of the Exchange Screening Parameter on the Performance of Screened Hybrid Functionals. *J. Chem. Phys.* **2006**, *125*, 224106.

(18) Ziman, J. M. *Principles of the Theory of Solid*; Cambridge University Press: Cambridge, **1971**.

(19) Mostofi, A. A.; Yates, J. R.; Lee, Y.-S.; Souza, I.; Vanderbilt, D.; Marzari, N. wannier90: A Tool for Obtaining Maximally-Localised Wannier Functions. *Comput. Phys. Commun.* **2008**, *178*, 685-699.

(20) Madsen, G. K. H. Automated Search for New Thermoelectric Materials: the Case of LiZnSb. *J. Am. Chem. Soc.* **2006**, *128*, 12140-12146.

(21) Wang, D.; Shi, W.; Chen, J.; Xi, J.; Shuai, Z. Modeling Thermoelectric Transport in Organic Materials. *Phys. Chem. Chem. Phys.* **2012**, *14*, 16505-16520.

(22) Shuai, Z.; Wang, D.; Peng, Q.; Geng, H. Computational Evaluation of Optoelectronic Properties for Organic/Carbon Materials. *Acc. Chem. Res.* **2014**, *47*, 3301-3309.

(23) Bardeen, J.; Shockley, W. Deformation Potentials and Mobilities in Non-Polar Crystals. *Phys. Rev.* **1950**, *80*, 72-80.

(24) Long, M.-Q.; Tang, L.; Wang, D.; Wang, L.; Shuai, Z. Theoretical Predictions of Size-Dependent Carrier Mobility and Polarity in Graphene. *J. Am. Chem. Soc.* **2009**, *131*, 17728-17729.

(25) Shi, W.; Chen, J.; Xi, J.; Wang, D.; Shuai, Z. Search for Organic Thermoelectric Materials with High Mobility: the Case of 2,7-Dialkyl[1]benzothieno[3,2-b][1]benzothiophene Derivatives. *Chem. Mater*. **2014**, *26*, 2669-2677.

(26) Shi, W.; Zhao, T.; Xi, J.; Wang, D.; Shuai, Z. Unravelling Doping Effects on PEDOT at the Molecular Level: from Geometry to Thermoelectric Transport Properties. *J. Am. Chem. Soc.* **2015**, *137*, 12929-12938.

(27) Shi, W.; Shuai, Z.; Wang, D. Tuning Thermal Transport in Chain-Oriented Conducting Polymers for Enhanced Thermoelectric Efficiency: A Computational Study. *Adv. Funct. Mater.* **2017**, *27*, 1702847-1702854.

(28) Baroni, S.; de Gironcoli, S.; Dal Corso, A.; Giannozzi, P. Phonons and Related Crystal Properties from Density-Functional Perturbation Theory. *Rev. Mod. Phys.* **2001**, *73*, 515-562.

(29) Marzari, N.; Mostofi, A. A.; Yates, J. R.; Souza, I.; Vanderbilt, D. Maximally Localized Wannier Functions: Theory and Applications. *Rev. Mod. Phys.* **2012**, *84*, 1419-1475.

(30) Hamann, D. R.; Schlüter, M.; Chiang, C. Norm-Conserving Pseudopotentials. *Phys. Rev. Lett.* **1979**, *43*, 1494-1497.

(31) Giannozzi, P.; Andreussi, O.; Brumme, T.; Bunau, O.; Nardelli, M. B.; Calandra, M.; Car, R.; Cavazzoni, C.; Ceresoli, D.; Cococcioni, M.; Colonna, N.; Carnimeo, I.; Corso, A. D.; Gironcoli, S. d.; Delugas, P.; R. A. DiStasio, J.; Ferretti, A.; Floris, A.; Fratesi, G.; Fugallo, G.; Gebauer, R.; Gerstmann, U.; Giustino, F.; Gorni, T.; Jia, J.; Kawamura, M.; Ko, H. Y.; Kokalj, A.; Küçükbenli, E.; Lazzeri, M.; Marsili, M.; Marzari, N.; Mauri, F.; Nguyen, N. L.; Nguyen, H. V.; Otero-de-la-Roza, A.; Paulatto, L.; Poncé, S.; Rocca, D.; Sabatini, R.; Santra, B.; Schlipf, M.; Seitsonen, A. P.; Smogunov, A.; Timrov, I.; Thonhauser, T.; Umari, P.; Vast, N.; Wu, X.; Baroni, S. Advanced Capabilities for Materials Modelling with Quantum ESPRESSO. *J. Phys. Condens Matter*. **2017**, *29*, 465901-465930.

(32) Poncé, S.; Margine, E. R.; Verdi, C.; Giustino, F. EPW: Electron–Phonon Coupling, Transport and Superconducting Properties Using Maximally Localized Wannier Functions. *Comput. Phys. Commun.* **2016**, *209*, 116-133.

(33) Fan, H. Y. Temperature Dependence of the Energy Gap in Semiconductors. *Phys. Rev.* **1951**, *82*, 900-905.

(34) Alvarez, S.; Vicente, R.; Hoffmann, R. Dimerization and Stacking in Transition-Metal Bisdithiolenes and Tetrathiolates. *J. Am. Chem. Soc.* **1985**, *107*, 6253-6277.

(35) Vogt, T.; Faulmann, C.; Soules, R.; Lecante, P.; Mosset, A.; Castan, P.; Cassoux, P.; Galy, J. A LAXS (large angle x-ray scattering) and EXAFS (extended x-ray absorption fine structure)

Investigation of Conductive Amorphous Nickel Tetrathiolato Polymers. *J. Am. Chem. Soc.* **1988**, *110*, 1833-1840.

(36) Mahan, G. D. Figure of Merit for Thermoelectrics. *J. Appl. Phys.* **1989**, *65*, 1578-1583.

(37) Tang, L.-P.; Tang, L.-M.; Geng, H.; Yi, Y.-P.; Wei, Z.; Chen, K.-Q.; Deng, H.-X. Tuning Transport Performance in Two-Dimensional Metal-Organic Framework Semiconductors: Role of the Metal d Band. *Appl. Phys. Lett.* **2018**, *112*, 012101-012105.

(38) Hsu, B. B.-Y.; Cheng, C.-M.; Luo, C.; Patel, S. N.; Zhong, C.; Sun, H.; Sherman, J.; Lee, B. H.; Ying, L.; Wang, M.; Bazan, G.; Chabinyc, M.; Brédas, J.-L.; Heeger, A. The Density of States and the Transport Effective Mass in a Highly Oriented Semiconducting Polymer: Electronic Delocalization in 1D. *Adv. Mater.* **2015**, *27*, 7759-7765.

(39) Auslender, M.; Hava, S. In *Springer Handbook of Electronic and Photonic Materials*; Kasap, S., Capper, P., Eds.; Springer International Publishing: Cham, 2017, p 1-1.

(40) Méndez, H.; Heimel, G.; Opitz, A.; Sauer, K.; Barkowski, P.; Oehzelt, M.; Soeda, J.; Okamoto, T.; Takeya, J.; Arlin, J.-B.; Balandier, J.-Y.; Geerts, Y.; Koch, N.; Salzmann, I. Doping of Organic Semiconductors: Impact of Dopant Strength and Electronic Coupling. *Angew. Chem. Int. Ed.* **2013**, *52*, 7751-7755.

(41) Xi, J.; Wang, D.; Yi, Y.; Shuai, Z. Electron-Phonon Couplings and Carrier Mobility in Graphynes Sheet Calculated Using the Wannier-Interpolation Approach. *J. Chem. Phys.* **2014**, *141*, 034704-034713.

(42) Tang, L.; Long, M.; Wang, D.; Shuai, Z. The Role of Acoustic Phonon Scattering in Charge Transport in Organic Semiconductors: A First-Principles Deformation-Potential Study. *Sci. China Ser. B-Chem.* **2009**, *52*, 1646-1652.

(43) Beleznay, F. B.; Bogar, F.; Szekeres, Z.; Ladik, J. Calculation of the Charge-Carrier Mobility of Polyguanylic Acid: The Simultaneous Effect of Stretching and Twisting. *J. Chem. Phys.* **2006**, *124*, 074708-074711.

(44) Long, M.; Tang, L.; Wang, D.; Li, Y.; Shuai, Z. Electronic Structure and Carrier Mobility in Graphdiyne Sheet and Nanoribbons: Theoretical Predictions. *ACS Nano* **2011**, *5*, 2593-2600.

(45) Neugebauer, P.; Orlita, M.; Faugeras, C.; Barra, A. L.; Potemski, M. How Perfect Can Graphene Be? *Phys. Rev. Lett.* **2009**, *103*, 136403-136406.

(46) Huang, X.; Sheng, P.; Tu, Z.; Zhang, F.; Wang, J.; Geng, H.; Zou, Y.; Di, C.-a.; Yi, Y.; Sun, Y.; Xu, W.; Zhu, D. A Two-Dimensional π–d Conjugated Coordination Polymer with Extremely High Electrical Conductivity and Ambipolar Transport Behaviour. *Nature Commun.* **2015**, *6*, 7408-7415.

(47) Prins, P.; Grozema, F. C.; Schins, J. M.; Patil, S.; Scherf, U.; Siebbeles, L. D. A. High Intrachain Hole Mobility on Molecular Wires of Ladder-Type Poly(p-Phenylenes). *Phys. Rev. Lett.* **2006**, *96*, 146601-146604.

(48) Liu, C.; Huang, K.; Park, W.-T.; Li, M.; Yang, T.; Liu, X.; Liang, L.; Minari, T.; Noh, Y.-Y. A Unified Understanding of Charge Transport in Organic Semiconductors: the Importance of Attenuated Delocalization for the Carriers. *Mater. Horiz.* **2017**, *4*, 608-618.

(49) Oberhofer, H.; Reuter, K.; Blumberger, J. Charge Transport in Molecular Materials: An Assessment of Computational Methods. *Chem. Rev.* **2017**, *117*, 10319-10357.

(50) Kang, K.; Watanabe, S.; Broch, K.; Sepe, A.; Brown, A.; Nasrallah, I.; Nikolka, M.; Fei, Z.; Heeney, M.; Matsumoto, D.; Marumoto, K.; Tanaka, H.; Kuroda, S.-i.; Sirringhaus, H. 2D Coherent Charge Transport in Highly Ordered Conducting Polymers Doped by Solid State Diffusion. *Nature Mater.* **2016**, *15*, 896-903.

(51) Vasseur, G.; Fagot-Revurat, Y.; Sicot, M.; Kierren, B.; Moreau, L.; Malterre, D.; Cardenas, L.; Galeotti, G.; Lipton-Duffin, J.; Rosei, F.; Di Giovannantonio, M.; Contini, G.; Le Fèvre, P.; Bertran, F.; Liang, L.; Meunier, V.; Perepichka, D. F. Quasi One-Dimensional Band Dispersion and Surface Metallization in Long-Range Ordered Polymeric Wires. *Nature Commun.* **2016**, *7*, 10235-10243.

(52) Noriega, R.; Rivnay, J.; Vandewal, K.; Koch, F. P. V.; Stingelin, N.; Smith, P.; Toney, M. F.; Salleo, A. A General Relationship between Disorder, Aggregation and Charge Transport in Conjugated Polymers. *Nature Mater.* **2013**, *12*, 1038-1044.

(53) Luo, C.; Kyaw, A. K. K.; Perez, L. A.; Patel, S.; Wang, M.; Grimm, B.; Bazan, G. C.; Kramer, E. J.; Heeger, A. J. General Strategy for Self-Assembly of Highly Oriented Nanocrystalline Semiconducting Polymers with High Mobility. *Nano Lett.* **2014**, *14*, 2764-2771.

(54) Cho, B.; Park, K. S.; Baek, J.; Oh, H. S.; Koo Lee, Y.-E.; Sung, M. M. Single-Crystal Poly(3,4-ethylenedioxythiophene) Nanowires with Ultrahigh Conductivity. *Nano Lett.* **2014**, *14*, 3321-3327.

(55) Yu, Y.; Junto, T.; Felix, H.; Yugo, O.; Junshi, S.; Wojciech, Z.; Martin, B.; Wojciech, P.; Hiroyuki, M.; Klaus, M.; Jun, T. Transition Between Band and Hopping Transport in Polymer Field‐Effect Transistors. *Adv. Mater.* **2014**, *26*, 8169-8173.

(56) Yamashita, Y.; Hinkel, F.; Marszalek, T.; Zajaczkowski, W.; Pisula, W.; Baumgarten, M.; Matsui, H.; Müllen, K.; Takeya, J. Mobility Exceeding 10 $cm^2/(V\cdot s)$ in Donor–Acceptor Polymer Transistors with Band-like Charge Transport. *Chem. Mater.* **2016**, *28*, 420-424.

(57) Lee, J.; Chung, J. W.; Kim, D. H.; Lee, B.-L.; Park, J.-I.; Lee, S.; Häusermann, R.; Batlogg, B.; Lee, S.-S.; Choi, I.; Kim, I. W.; Kang, M. S. Thin Films of Highly Planar Semiconductor

Polymers Exhibiting Band-like Transport at Room Temperature. *J. Am. Chem. Soc.* **2015**, *137*, 7990-7993.

(58) Salzmann, I.; Heimel, G.; Duhm, S.; Oehzelt, M.; Pingel, P.; George, B. M.; Schnegg, A.; Lips, K.; Blum, R.-P.; Vollmer, A.; Koch, N. Intermolecular Hybridization Governs Molecular Electrical Doping. *Phys. Rev. Lett.* **2012**, *108*, 035502-035506.

(59) Kambe, T.; Sakamoto, R.; Hoshiko, K.; Takada, K.; Miyachi, M.; Ryu, J.-H.; Sasaki, S.; Kim, J.; Nakazato, K.; Takata, M.; Nishihara, H. π-Conjugated Nickel Bis(dithiolene) Complex Nanosheet. *J. Am. Chem. Soc.* **2013**, *135*, 2462-2465.

(60) Bubnova, O.; Khan, Z. U.; Wang, H.; Braun, S.; Evans, D. R.; Fabretto, M.; Hojati-Talemi, P.; Dagnelund, D.; Arlin, J.-B.; Geerts, Y. H.; Desbief, S.; Breiby, D. W.; Andreasen, J. W.; Lazzaroni, R.; Chen, W. M.; Zozoulenko, I.; Fahlman, M.; Murphy, P. J.; Berggren, M.; Crispin, X. Semi-Metallic Polymers. *Nature Mater.* **2014**, *13*, 190-194.

(61) Reynolds, J. R.; Chien, J. C. W.; Lillya, C. P. Intrinsically Electrically Conducting Poly(metal tetrathiooxalates). *Macromolecules* **1987**, *20*, 1184-1191.

(62) Menon, A. K.; Wolfe, R. M. W.; Marder, S. R.; Reynolds, J. R.; Yee, S. K. Systematic Power Factor Enhancement in n-Type NiETT/PVDF Composite Films. *Adv. Funct. Mater.* **2018**, *28*, 1801620-1801626.

(63) Tsao, H. N.; Cho, D. M.; Park, I.; Hansen, M. R.; Mavrinskiy, A.; Yoon, D. Y.; Graf, R.; Pisula, W.; Spiess, H. W.; Müllen, K. Ultrahigh Mobility in Polymer Field-Effect Transistors by Design. *J. Am. Chem. Soc.* **2011**, *133*, 2605-2612.

(64) Basescu, N.; Liu, Z. X.; Moses, D.; Heeger, A. J.; Naarmann, H.; Theophilou, N. High Electrical Conductivity in Doped Polyacetylene. *Nature* **1987**, *327*, 403-405.

(65) Naarmann, H.; Theophilou, N. New Process for the Production of Metal-like, Stable Polyacetylene. *Synth. Met.* **1987**, *22*, 1-8.

(66) Fritzsche, H. A General Expression for the Thermoelectric Power. *Solid State Commun.* **1971**, *9*, 1813-1815.

(67) Kim, G. H.; Shtein, M.; Pipe, K. P. Thermoelectric and Bulk Mobility Measurements in Pentacene Thin Films. *Appl. Phys. Lett.* **2011**, *98*, 093303-093305.

For Table of Contents Only